THE JOURNAL OF PHYSICAL CHEMISTRY C

Article

pubs.acs.org/JPCC

Probing the Dependence of Electron Transfer on Size and Coverage in Carbon Nanotube–Quantum Dot Heterostructures

Lei Wang,[†] Jinkyu Han,[‡] Yuqi Zhu,[§] Ruiping Zhou,[§] Cherno Jaye,[∥] Haiqing Liu,[†] Zhuo-Qun Li,[⊥] Gordon T. Taylor,[⊥] Daniel A. Fischer,[∥] Joerg Appenzeller,[§] and Stanislaus S. Wong*[,†,‡]

[†]Department of Chemistry, State University of New York at Stony Brook, Stony Brook, New York 11794-3400, United States

[‡]Condensed Matter Physics and Materials Sciences Department, Brookhaven National Laboratory, Building 480, Upton, New York 11973, United States

[§]Department of Electrical and Computer Engineering and Birck Nanotechnology Center, Purdue University, West Lafayette, Indiana 47907, United States

[∥]Material Measurement Laboratory, National Institute of Standards and Technology, Gaithersburg, Maryland 20889, United States

[⊥]School of Marine and Atmospheric Sciences, State University of New York at Stony Brook, Stony Brook, New York 11794-5000, United States

Supporting Information

ABSTRACT: As a model system for understanding charge transfer in novel architectural designs for solar cells, double-walled carbon nanotube (DWNT)–CdSe quantum dot (QD) (QDs with average diameters of 2.3, 3.0, and 4.1 nm) heterostructures have been fabricated. The individual nanoscale building blocks were successfully attached and combined using a hole-trapping thiol linker molecule, i.e., 4-mercaptophenol (MTH), through a facile, noncovalent $\pi-\pi$ stacking attachment strategy. Transmission electron microscopy confirmed the attachment of QDs onto the external surfaces of the DWNTs. We herein demonstrate a meaningful and unique combination of near-edge X-ray absorption fine structure (NEXAFS) and Raman spectroscopies bolstered by complementary electrical transport measurements in order to elucidate the synergistic interactions between CdSe QDs and DWNTs, which are facilitated by the bridging MTH molecules that can scavenge photoinduced holes and potentially mediate electron redistribution between the conduction bands in CdSe QDs and the C 2p-derived states of the DWNTs. Specifically, we correlated evidence of charge transfer as manifested by (i) changes in the NEXAFS intensities of π^* resonance in the C K-edge and Cd M_3-edge spectra, (ii) a perceptible outer tube G-band downshift in frequency in Raman spectra, as well as (iii) alterations in the threshold characteristics present in transport data as a function of CdSe QD deposition onto the DWNT surface. In particular, the separate effects of (i) varying QD sizes and (ii) QD coverage densities on the electron transfer were independently studied.

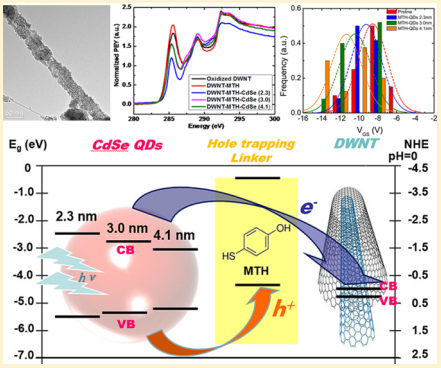

INTRODUCTION

Carbon nanotube (CNT)–quantum dot (QD) heterostructures, which merge the favorable charge transport properties of CNTs with the interesting size-tunable optoelectronic properties of QDs into an integrated whole, represent not only a conceptually unusual architectural paradigm but also a practically functional nanocomposite in the field of photovoltaic cells.[1−5] In our group, we have successfully demonstrated various synthetic methods including covalent attachment, $\pi-\pi$ stacking, as well as an in situ route toward the simple, site-selective, and coverage-controllable synthesis of single-walled carbon nanotube (SWNT), double-walled carbon nanotube (DWNT), and multiwalled carbon nanotube (MWNT)–CdSe/CdTe quantum dot (QD) conjugates.[6−8]

In this work, we have specifically chosen to use DWNTs as opposed to SWNTs. One rationale is that the acid purification process developed to remove the metal catalysts and amorphous carbon impurities from the pristine carbon nanotubes often involves the breaking of the sp^2 structure of the nanotube sidewall, thereby diminishing the attractive electronic transport characteristics we seek to exploit when utilizing SWNTs. Moreover, with DWNTs, consisting of two coaxial tubules, we can selectively functionalize the outer tube while retaining the desirable electronic properties of the inner tube.[1]

Nevertheless, the crucial step in understanding the nature of QD-based photovoltaic cells involves control over the effective interfacial charge transfer, which is often inefficient because of the spatial confinement of the electron and the hole to the interior of the QDs as well as to the unavoidable recombination

Received: September 5, 2015
Revised: October 28, 2015
Published: November 16, 2015

DOI: 10.1021/acs.jpcc.5b08681
J. Phys. Chem. C 2015, 119, 26327−26338

process caused by the Coulombic interaction.[9] This issue can be potentially tackled by rational chemical design. Specifically, by properly choosing linker molecules and the subsequent chemical modification of the external surfaces of these QDs through a ligand exchange reaction in order to passivate surface defects, we can do much toward controlling surface-related emission and reducing recombination losses.[10] In fact, the fabrication of conductive QD films for optimum operation within a solar cell regime often relies on replacing the long alkyl ligands used in colloidal QD synthesis with short organic bidentate linkers, such as either ethanedithiol or 3-mercaptopropionic acid (MPA), for instance.[11,1213] These specific short bidentate linkers not only reduce the interdot separation to less than the carrier tunneling distance, thereby facilitating exciton dissociation and enabling carrier transport toward the collecting contacts,[14,15] but also serve as a bridge with which to connect QDs with CNTs through either covalent or noncovalent attachment strategies.[6,16]

The specific linker molecule we have deliberately chosen here is 4-mercaptophenol (MTH) with the terminal thiol−SH group, possessing a strong affinity for Cd sites on the QD surface. The presence of the aromatic aryl ring moiety within the MTH molecule can be manipulated in order to initiate heterostructure formation through facile noncovalent $\pi-\pi$ stacking interactions with the CNT sidewalls. It has been previously reported that the presence of thiol functional groups within MTH can serve as "hole-scavengers" and thereby act as effective acceptors for photogenerated holes from the CdSe QDs. These photogenerated holes from CdSe QDs can efficiently convert thiols into disulfides by means of a photocatalytic reaction.[17,18]

Because of the conduction band alignment of CdSe QDs with either adjacent DWNTs or metal oxides, interfacial electron transfer has been extensively studied.[19−21] In terms of metal oxides, Hansen et al. detected photoinduced electron transfer from CdSe QDs to ZnO nanorods connected together using three small saturated carboxythiol linkers.[21] Moreover, Hines et al. have reported on electron tunneling from CdSe to TiO_2, a process facilitated by various thiol linkers, which served as energy barriers due to their elevated 'lowest unoccupied molecular orbital' (i.e., LUMO) levels as compared with both QDs and TiO_2.[22] Additional examples exist. For example, Weaver et al. investigated the photoinduced electron and hole transfer within a complex nanocomposite, consisting of CNTs, thiol derivatives of perylene compounds, and CdSe QDs.[23] Herein, in our experiments, because the bridging MTH linker molecules maintain a higher LUMO level as compared with both CdSe QDs and DWNTs, the linkers can be viewed as creating an energetic barrier located at the interface between the constitutent quantum dots and nanotubes within our as-prepared heterostructures. Therefore, electrons from QDs need to tunnel through the linkers themselves prior to their localization onto adjoining DWNTs, whereas the associated holes are expected to be trapped by the terminal thiol groups inherent to the MTH.

Understanding of interfacial charge transport mechanisms is therefore essential toward realizing the optimal design and construction of high-performance QD-based solar energy conversion systems.[24] As a means of probing interfacial interactions among nanocomposites, the use of near-edge X-ray absorption fine structure (NEXAFS) spectroscopy has been extensively investigated,[25−28] because it is element-specific and also very sensitive to the local chemical environment. In particular, *NEXAFS* analyzes the occupancy of the low-lying unoccupied electronic states associated with the absorbing atom, and as such, in our context, can be used to investigate the contribution of electron as opposed to hole transfer within our heterostructures.[29]

With respect to relevant, prior results, by analyzing the Sn $M_{5,4}$ edge, O *K*-edge, and C *K*-edge within systems composed of crystalline SnO_2 nanoparticles (NPs) connected to CNTs, it was noted that this interaction involved a charge redistribution between C 2p-derived states with the valence and conduction bands in SnO_2 NPs via an interfacial interaction facilitated by the oxidative treatment of the CNTs, prior to composite formation.[30] Additional examples abound. Koroteev et al. reported on a decrease of the π^* resonance intensity in the C *K*-edge spectrum upon MoS_2 deposition onto the CNT surface, signifying the likelihood of charge transfer between the two components.[31] Yueh et al. investigated the local electronic structure associated with "Fe-catalyzed and stabilized" CNTs of various diameters and measured an enhancement of the C *K*-edge coupled with a corresponding reduction of the Fe L_3-edge features, all of which were indicative of a charge transfer taking place from C 2p to Fe 3d orbitals.[32]

In terms of charge-transfer properties, the *Raman* spectra of both constituent CNTs and the resulting heterostructures have been collected with a focus toward analyzing and understanding relative changes in certain distinctive bands associated with CNTs. Specifically, the high-frequency Raman-active vibrations of sp^2 carbon are sensitive to chemical doping.[33] Hence, by studying the resonance Raman spectra of DWNTs, doped with electron donors and acceptors, we can gain insight into chemical means of modulating CNT electronic properties.[34−37] In effect, shifts in the Raman frequencies for the tangential G^+ modes and the corresponding alterations in their intensities can provide for direct evidence for charge transfer between CNTs and the dopants themselves.[38] For example, Li et al. have reported a large downshift of the G-band, which was suggestive of substantial electron transfer between Fe atoms and DWNTs.[39]

In order to monitor the charge carrier mobility in our heterostructures, *electrical transport* measurements have been collected by constructing field effect transistor (FET) devices. Owing to their suitable direct bandgap (E_g = 1.74 eV), which yields a measurable response upon exposure to visible light, CdSe QDs have attracted extensive attention as promising candidates for applications in photovoltaic and photoelectronic devices.[40,41] Moreover, CNTs also yield respectable field-effect mobility and therefore represent a promising architecture for electronic devices.[42] There have been reports focusing on FETs, created using CNT−QD heterostructures. For example, Zhao et al. noted that CdSe QDs formed in situ on the carbon nanobelt matrix could give rise to the formation of a nanoscale *p*−i−*n* junction, possessing *p*-type conductivity with hole mobility values as high as 1.4×10^4 $cm^2\,V^{-1}\,s^{-1}$.[43]

Therefore, it is interesting to note that while NEXAFS, Raman, and electrical transport measurements have been separately applied as tools to investigate charge transfer in various types of nanotube-based heterostructure motifs for years, there have been comparatively fewer papers published about utilizing these unique characterization protocols within the context of DWNT−QD heterostructures in order to study the nature of interfacial charge transfer. There have been even fewer deliberative and systematic efforts (either qualitatively or quantitatively) to use a cumulative combination of *all* of these

DOI: 10.1021/acs.jpcc.5b08681
J. Phys. Chem. C 2015, 119, 26327−26338

techniques in CNT−QD systems with the focus on probing and correlating the effect of varying QD sizes and coverage densities with the resulting charge-transfer properties of as-prepared nanocomposites. We are in fact the first to do so.

Hence, in the current paper, we focus on gaining fundamental insights into charge-transfer behavior across nanoscale interfaces in composite heterostructures as a function of QD size and coverage density. Specifically, our efforts are directed toward comparing and understanding charge-transfer behavior, i.e., specifically electron-transfer trends, at the interfaces of a number of different DWNT−CdSe QD heterostructures, possessing various QD average diameters of 2.3, 3.0, and 4.1 nm, respectively, created through the mediation of 4-mercaptophenol (MTH) using a noncovalent $\pi-\pi$ stacking attachment approach. The structure, morphology, and specifically the QD coverage density on the DWNT surface were characterized by transmission electron microscopy (TEM). Meanwhile, complementary data from NEXAFS and Raman spectroscopies coupled with electrical transport measurements were acquired on both constituent CNTs and the resulting heterostructures with the aim of understanding the nature of nuanced but reproducible data trends, governing charge transfer (and specifically electron tunneling) from QDs, characterized by various sizes and coverage densities, to DWNTs within composite architectures.

EXPERIMENTAL SECTION

Materials. DWNTs were acquired from Helix Material Solutions. As for the CdSe QD synthesis and the subsequent ligand-exchange process, hexadecylamine (HDA) (90%), selenium powder (100 mesh, 99.5%), and 4-mercaptophenol (MTH) (97%) were procured from Aldrich. Tri-*n*-octylphosphine oxide (TOPO) (99%), stearic acid (97%), cadmium oxide (CdO) (99%), and tri-*n*-butylphosphine (TBP) (95%) were purchased from Acros Organics. Tri-*n*-octylphosphine oxide (TOPO) (90%) was obtained from Alfa Aesar.

Synthesis. *Purification of DWNTs.* Specifically, 50 mg of pristine DWNTs containing amorphous carbon impurities (Figure S1A) were dispersed in 8 M diluted HNO_3 by sonication and then heated to 95 °C for 20 h to remove extraneous metal catalysts and carbonaceous impurities. The resulting purified and oxidized DWNTs (pDWNTs in Figure S1B) were filtered through a 200 nm polycarbonate membrane (Millipore), thoroughly washed with excess water, and dried at 80 °C for 18 h.

Synthesis of CdSe QDs and Ligand-Exchange Processes. CdSe QDs with various sizes have been prepared, according to a well-known protocol, as previously described.[44] Depending on the targeted QD sizes, different sources of TOPO were chosen with minor modifications of the reaction algorithm. For example, to create QDs possessing average particle diameters of 2.3 and 3.0 nm, TOPO from Alfa Aesar was used, with reaction times of 15 s and 20 min, respectively. As for the synthesis of QDs with average diameters of 4.1 nm, TOPO from Acros Organics was utilized with reaction times of ∼100 s. Ultraviolet (UV)−visible spectra (Figure S2A) confirmed the size-tunable absorption of as-prepared CdSe QDs; powder X-ray diffraction data (Figure S2B) proved that the crystal structure of our QDs was in fact würtzite. In addition, the ligand exchange process was carried out on as-prepared CdSe QDs to replace the original TOPO and HDA capping agents with the MTH ligand moiety.

In a typical experiment, 0.1 mmol of MTH was dissolved in 2 mL of methanol and added drop-wise to a suspension of as-prepared, TOPO/HDA-capped CdSe QDs (0.04 mmol) in 4 mL of hexane ([Ligands]/[QDs] = 25). Under dark conditions, the methanolic solution mixture was stirred for 30 min, until the CdSe QDs could be subsequently precipitated upon completion of the ligand exchange process. As-generated MTH-capped CdSe QDs were then collected by centrifugation and subsequently washed with a methanol and chloroform mixture (with a volume ratio of 1:8) at 9000 rpm for 5 min for three successive times. The resulting QDs were ultimately re-dispersed in dimethyl sulfoxide (DMSO) for additional characterization. The presence of MTH ligands on the external CdSe QD surfaces was expected after the ligand exchange reaction, and was subsequently confirmed by Fourier transfrom infrared analysis, as shown in Figure S3.

Synthesis of DWNT−MTH-Capped CdSe QD Heterostructures by $\pi-\pi$ Stacking. In a typical run, as illustrated in Scheme 1, 1 mg of pDWNT was dispersed in 10 mL of DMSO

Scheme 1. Synthetic Route Associated with the Noncovalent Attachment of MTH-Functionalized CdSe QDs onto Underlying DWNT Frameworks

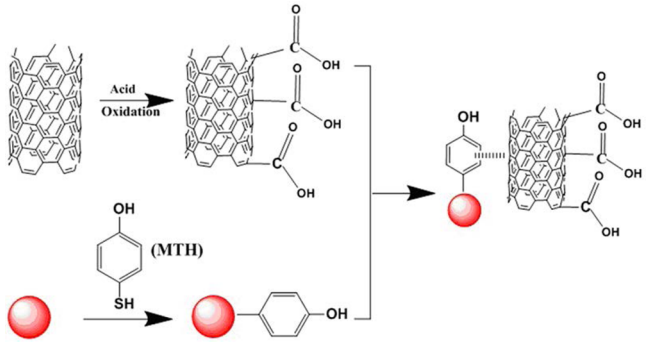

by sonication followed by the addition of 2 mL of MTH-capped CdSe QDs (0.004 mmol) in DMSO in a drop-wise manner. The resulting mixture was further sonicated for 10 min. Upon completion of the reaction, the solution was filtered using 200 nm polycarbonate membranes (Millipore), extensively washed with distilled water and ethanol to remove the excess free-standing CdSe QDs, and ultimately stored at 4 °C prior to further measurements.

Characterization. Samples were thoroughly characterized using a number of different complementary structural methodologies, including transmission electron microscopy, UV−visible spectra (UV−visible), and powder X-ray diffraction (XRD) as well as a suite of Raman and near-edge X-ray absorption fine structure spectroscopies. We strengthened our interpretation with additional complementary electrical transport measurements.

Electron Microscopy. Low-magnification TEM images were obtained at an accelerating voltage of 120 kV on the JEOL JEM-1400 instrument, with a 2048 × 2048 Gatan CCD Digital Camera. High-resolution TEM (HR-TEM) images coupled with selected area electron diffraction (SAED) patterns were recorded using a JEOL JEM-3000F microscope, equipped with a Gatan image filter (GIF) spectrometer and operated at an accelerating voltage of 300 kV. Specimens for all of these TEM experiments were prepared by dispersing the as-prepared product in ethanol, sonicating for 2 min to ensure adequate

DOI: 10.1021/acs.jpcc.5b08681
J. Phys. Chem. C 2015, 119, 26327−26338

dispersion of the nanostructures, and dipping one drop of solution onto a 300 mesh Cu grid, coated with a lacey carbon film.

X-ray Diffraction. Crystallographic information on CdSe QDs was obtained by using powder XRD. To analyze these materials, as-prepared samples were sonicated, dispersed in ethanol for about 2 min, and finally air-dried upon deposition onto glass slides. Diffraction patterns for all of these materials were collected using a Scintag diffractometer, operating in the Bragg configuration with Cu Kα radiation (λ = 1.54 Å) and scanning in the range from 20 to 80° at a rate of 0.25° per minute.

UV−Visible Spectra. UV−visible spectra were collected at high resolution using a Thermospectronics UV1 instrument as dispersions within quartz cells maintaining a 10 mm path length. Specifically, as-prepared QDs were suspended in hexane, and the acquired data were corrected to account for, and more precisely to subtract away, the solvent background.

NEXAFS. Carbon *K*-, oxygen *K*-, and cadmium M_3-edge NEXAFS measurements were carried out at the NIST U7A beamline at the National Synchrotron Light Source at Brookhaven National Laboratory. NEXAFS spectra were obtained using a horizontally polarized X-ray beam incident at 55° (i.e., magic angle) and a channeltron electron multiplier equipped with a variable entrance grid bias. For the various elements studied, the entrance grid bias was set to −150 V to enhance surface sensitivity and reduce the low-energy electron background. A toroidal spherical grating monochromator, composed of a 600 lines/mm grating for the C *K*-edge data as well as a 1200 lines/mm grating for the Cd M_3 and O *K*-edges, was used. Slit openings of 30 × 30 μm^2 along the beamline provided an energy resolution of ∼0.1 eV for all spectra. An electron flood gun set at 60 μA was used to mitigate surface charging.

The PEY signals were normalized to the incident beam intensity using the photoemission signal from a freshly evaporated Au mesh located along the incident beam path. The spectra were energy-calibrated using the photoemission current from an amorphous carbon mesh also located along the path of the incident beam. Spectra were calibrated and normalized using standard routines from the Athena software.[45]

Raman. Raman spectra were collected from our samples using a Renishaw inVia high-resolution confocal Raman microscope outfitted with a Leica DM2500 upright microscope using a 514.5 nm (2.41 eV) in-line laser. The microscope stage was fitted with an automated *xyz*-motorized stage. Wavelength and intensity calibrations were completed by using an internal silicon standard based upon a reference peak at 520 cm^{-1}.

Spectra from the samples were collected using an 1800 line/mm grating, resulting in a spectral resolution of ∼0.5 cm^{-1}, with a 10 s integration time per spectrum using a CCD array. Raw spectra were subsequently processed and analyzed using WiRE 4.1 software. Baselines were subtracted from all of the spectra, and the integrated spectral areas were normalized to an area of 1. The resulting peaks were then fitted with four Lorentzian curves to determine the peak position, integrated areas (intensity), and peak widths.

Electrical Transport. Electrical transport measurements have been used to complement the NEXAFS and Raman data as well as to gain additional insights into the impacts of QD size and coverage density. To this extent, devices have been fabricated on a highly *p*-doped silicon substrate with a 90 nm silicon dioxide layer on top. The substrate is used in our measurements as the gate electrode. Next, carbon nanotubes either with or without functionalization are spun out of solution onto the substrate. To contact only a single DWNT and not a network of DWNTs, an e-beam writing approach is utilized that identifies the position of tubes relative to pre-defined alignment marks. Source−drain contact formation is accomplished after the e-beam step through metal deposition and lift-off of titanium/gold (30 nm/30 nm) metal films. A probe station set up in conjunction with a parameter analyzer is then used to determine the current through the device, I_{DS}, as a function of drain, V_{DS}, and gate voltage, V_{GS}. To reduce any potential hysteresis effects on the device characteristics, a pulse measurement setup is employed. In a pulse measurement, the Hewlett-Packard (HP) parameter analyzer is turned off between each data point acquisition instead of being operated continuously. In total, more than 180 discrete and distinctive double-wall carbon nanotube (DWNT) field-effect transistors (FETs) were characterized in this fashion, giving rise to decent overall statistics, which has allowed us to observe trends between variously treated devices in spite of the presence of unavoidable device-to-device variations arising from different DWNT chiralities and diameters as well as general experimental irreproducibilities. All data presented in this article were obtained at room-temperature under a vacuum atmosphere of about 10^{-5} Torr.

RESULTS AND DISCUSSION

With the amount of DWNTs and the concentration of the MTH-capped CdSe QD solution kept constant in order to ensure data reliability, the resulting DWNT−MTH-capped CdSe QD heterostructures, incorporating average QD diameters measuring 2.3, 3.0, and 4.1 nm, respectively, were generated by utilizing a facile noncovalent $\pi-\pi$ stacking strategy (Scheme 1). TEM was utilized to characterize the QD sizes and coverage densities on the DWNT surface in the resulting heterostructures. Meanwhile, charge transfer (and specifically electron tunneling) from QDs with various sizes and coverage densities to DWNTs in heterostructures was probed using NEXAFS and Raman spectroscopies coupled with electrical transport measurements.

Electron Microscopy Studies. Low-magnification TEM data in Figure 1 highlighted the formation of all three heterostructures, formed by $\pi-\pi$ stacking, with the presence of QDs clearly visible on the outer surfaces of our purified DWNT bundles, created through the mediation of the MTH linker. On the basis of statistical measurements of 20 distinctive and discrete as-formed DWNT−QD bundles within each heterostructure sample, the corresponding average coverage density was found to be 14 ± 10 dots for MTH-capped QDs, possessing diameters of 2.3 ± 0.4 nm (Figure 1A); 16 ± 8 dots for MTH-capped QDs, with diameters of 3.0 ± 0.4 nm (Figure 1B); and 27 ± 5 dots for MTH-capped QDs, measuring 4.1 ± 0.6 nm in diameter (Figure 1C), respectively. All data were acquired on typical DWNT bundles with lengths of 100 nm and diameters of 20 nm.

This average coverage density of CdSe QDs immobilized onto the DWNT surface was estimated by dividing the total number of QDs attached onto the CNT surface by the corresponding length of the DWNTs normalized to 100 nm intervals. We found that the 4.1 nm CdSe QDs evinced a notably higher coverage density (almost two times) as compared with their 2.3 and 3.0 nm diameter analogues, possibly due to the presence of additional ligand molecules at

DOI: 10.1021/acs.jpcc.5b08681
J. Phys. Chem. C 2015, 119, 26327−26338

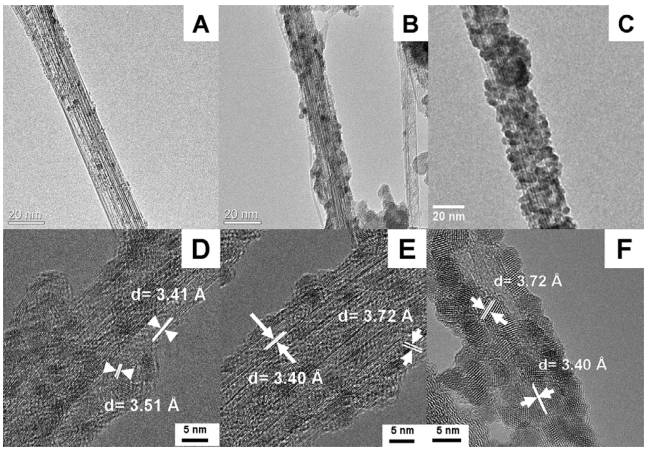

Figure 1. (A–C) TEM and (D–F) HRTEM images of DWNT–MTH-capped CdSe QD (with average constituent QD diameters of 2.3, 3.0, and 4.1 nm, respectively) heterostructures, synthesized by a noncovalent strategy, taking advantage of π–π stacking effects.

the surface, which would have contributed to more effective bonding with the underlying DWNT framework.

The corresponding HRTEM images in Figure 1D–F further confirmed the successful chemical conjugation of DWNTs with CdSe QDs. Lattice fringes associated with CdSe QDs as well as with the interface between the QDs and the DWNT surface were clearly discernible. Specifically, the measured 3.51 and 3.72 Å values corresponded to the *d*-spacings of the (002) and (100) lattice planes of the hexagonal phase of CdSe QDs, respectively, whereas the measured 3.41 Å spacing could be ascribed to the interlayer spacing between the graphitic layers within the DWNT themselves.

NEXAFS Spectra. The C *K*-edge and O *K*-edge spectra of the pristine and oxidized DWNTs (Figure S4A,B) were consistent with the successful purification and functionalization of DWNTs by acid treatment which generated oxygenated functionalities, e.g., –COOH groups, on their external surfaces (see detailed analysis in the Supporting Information on the identities of a number of peaks observed in both the carbon and oxygen *K*-edge data). The C and O *K*-edge NEXAFS spectra of the DWNTs, of the DWNT–MTH control sample, and of the DWNT–MTH-capped CdSe QD heterostructures are shown in panels A and B of Figure 2, respectively, whereas the Cd M_3-edge spectra of free-standing MTH-capped CdSe QDs as well as of all three DWNT–MTH-capped CdSe QD heterostructures are highlighted in Figure 3.

Explanation of Physical Meaning of Edge Data. Specifically, the C *K*-edge spectral features arise from dipole transitions from C 1s core states to 2p-derived electronic states. The sharp peak at around 285.4 eV represents a C 1s to a C=C 2p π^* transition; the broad peak at 292–294 eV is composed of three C 1s to C–C σ^* transitions.[28,46] Furthermore, the peaks at ~288.1 and ~289.1 eV can be attributed to the π^* C=O and σ^* states, respectively, associated with C–O functionalities.[27,29] Moreover, the areas under resonance (or peak intensity) of these π^* and σ^* features are approximately proportional to the electronic density of the unoccupied C 2p-derived states, whereas the increased intensities of these features can be correlated either with the increased numbers of unoccupied C 2p orbitals or with a charge-transfer process taking place between the C 2p orbital and the dopant at the interface.[28,30,32]

Two well-separated absorption features are observed in the O *K*-edge with a sharp peak located at 531.8 eV and a broader peak centered at around 539–546 eV. The feature at ~531 eV can be assigned to transitions from the O 1s core levels to π^* C=O states derived from carboxylic acid moieties, whereas the broad absorption feature centered at around 539–546 eV can be attributed to the superposition of transitions from the O 1s core levels to the final states possessing σ^* symmetry, localized on the O–H, C–O, and C=O bonds. The small peak at ~534.6 eV likely derives from the –OH π^* transition associated with carboxylic acid species.[26,47,48]

The Cd M_3 edge originates from transitions between the Cd 3p initial state and unoccupied 5s states. The projected electronic density of states (DOS) generated from theory demonstrates that the bottom of the conduction band of CdSe is composed of Cd 5s states. If the bottom of the CdSe conduction band were to shift by an energy interval, ΔE_c, then the corresponding M_3 absorption edge would shift by an equivalent amount, thereby representing the quantum confinement-induced shift in the conduction band.[49,50] Although the *M* edges are known to suffer from weak signals and a large background[49] by contrast with the Cd L_3 edge, the former can be readily probed within the operational energy range (180–1200 eV) of the U7A beamline. Therefore, to render these M_3 edges useful for quantitative analysis, we collected multiple replicates of the spectra and increased data integration times to obtain higher signal-to-noise ratios and therefore data interpretability.

Actual Results Obtained. On the basis of the C *K*-edge NEXAFS analysis (Figure 2A), several features are worthy of

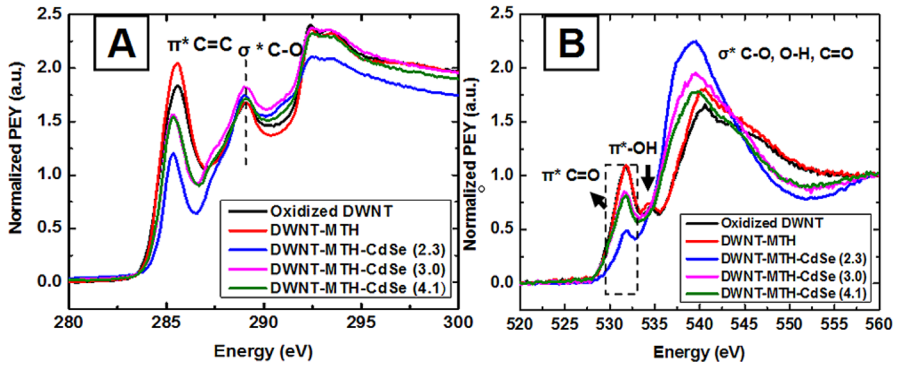

Figure 2. C *K*-edge (A) and O *K*-edge (B) spectra of oxidized DWNTs (black), DWNT–MTH composite control samples (red), and DWNT–MTH-capped CdSe QD (with constituent QD average diameters of 2.3 nm (blue), 3.0 nm (pink), and 4.1 nm (green)) heterostructures.

DOI: 10.1021/acs.jpcc.5b08681
J. Phys. Chem. C 2015, 119, 26327–26338

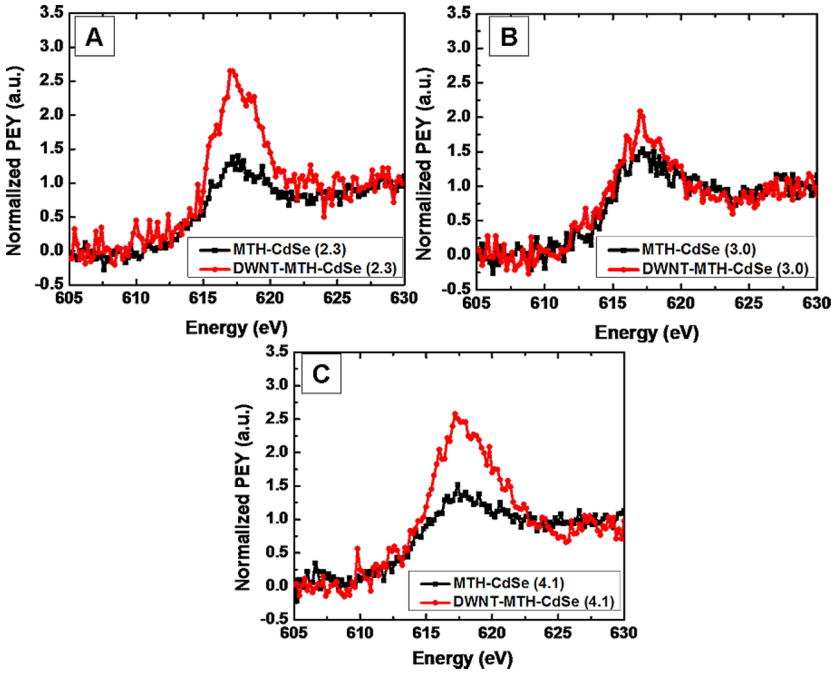

Figure 3. Cd M_3-edge spectra of MTH-functionalized CdSe QDs (black) and of DWNT−MTH-capped CdSe QD (red; with average constituent QD diameters of (A) 2.3 nm, (B) 3.0 nm, and (C) 4.1 nm) heterostructures.

note. First, the π^* transition intensity, which reflects the unoccupied DOS corresponding to π^* character, is enhanced when MTH linkers were attached onto oxidized DWNTs, which might be due to the presence of the sp^2 carbon from the aromatic MTH linker. This π^* transition intensity is subsequently strongly reduced within DWNT−MTH-capped CdSe QD heterostructures; the composites incorporating 2.3 nm diameter QDs give rise to the largest observed reduction, suggestive of possible electron transfer from CdSe conduction bands to the C 2p-derived π^* states.

Second, the appearance of a slightly enhanced C *K*-edge peak at ∼289 eV coupled with shoulder features near this peak within the heterostructures, as compared with the DWNT−MTH nanohybrid control alone, suggests the presence of slightly perturbed bonding between carbon and oxygen after the QD deposition process. That is, the presence of an oxidized C environment at the interface of the heterostructures may result in a localized and higher density of the unoccupied state possessing C 2p character, thereby indicating that DWNTs may have the opportunity of possibly back-donating a small amount of charge to the immobilized CdSe QDs through the mediation of Cd−O−C bonding.[28,51]

In the O *K*-edge data (Figure 2B), the C═O π^* transition intensity appears to be suppressed in all three heterostructures after the QD deposition as compared with the DWNT−MTH control sample. The heterostructure incorporating the smallest 2.3 nm diameter QDs gives rise to the strongest reduction in the C═O π^* transition, suggesting that the carbonyl oxygen atom within the carboxylic group on the surface of the DWNTs is withdrawing charge after QD deposition. By comparison, the C−O or −OH σ^* transition intensity is apparently enhanced the most in the heterostructure incorporating 2.3 nm diameter QDs, accordingly signifying that the oxygen atoms in the −OH and C−O bonds from the MTH ligands are donating charge.

We found that all three DWNT−MTH-capped CdSe QD heterostructures evince enhanced intensities of the Cd M_3-edge relative to that of free-standing MTH-capped CdSe QDs (Figure 3), thereby implying an increased level of unoccupied DOS in the conduction band of CdSe and providing for direct evidence of an electron-transfer process taking place from CdSe QDs to DWNTs. By analogy with the C and O *K*-edge features previously discussed, we noted that the heterostructure incorporating 2.3 nm diameter QDs exhibited the largest enhancement of the peak intensity, an observation consistent with the potential for the largest amount of electron transfer therein.

All NEXAFS spectra have yielded spectroscopic evidence that charge redistribution involving the CdSe QDs and the underlying DWNTs likely has occurred. Specifically, upon close inspection of the C and O *K*-edge together with the Cd M_3-edge data, these entailed (i) an intensity reduction in the π^* C═O and −OH signal of the O *K*-edge and the π^* C═C response of the C *K*-edge transitions coupled with (ii) an intensity enhancement in the Cd M_3-edge as well as the σ^* C−O or −OH signal associated with the O *K*-edge. Hence, it is plausible to propose a possible directional electron-transfer process, as follows. Upon excitation, the electrons migrate from the conduction band of the CdSe QDs to the π^* states of the DWNT C═C carbonaceous network as well as to the C═O π^* states of surface carboxylic acid functional moieties. This charge interaction was mediated between the $\pi-\pi$ conjugated system associated with the DWNTs and the MTH-capped CdSe QDs, as manifested in discernible but interpretable changes.

Therefore, we have shown that the DWNT−MTH-capped CdSe QD heterostructures incorporating the smallest 2.3 nm diameter QDs gives rise to the largest amount of electron transfer, an observation which can be potentially explained by the Marcus theory, which is commonly used to describe the interfacial charge-transfer process and to quantitatively probe the dependence of the transfer rate on the driving force.[52−54] Previous studies have indicated that electron transfer from

DOI: 10.1021/acs.jpcc.5b08681
J. Phys. Chem. C 2015, 119, 26327−26338

photoexcited QDs lies in the so-called "normal" region, where the charge-transfer rate increases with and is proportional to the driving force.[55,56] For example, the Kamat group reported[57] that by systematic reduction of the QD size, the electron transfer from CdSe QDs to the adjoining TiO_2 particles could be enhanced, and it was subsequently concluded that this transfer resides within the "normal" region of Marcus theory.

A potential charge-transfer model for our DWNT−MTH-capped CdSe QD systems, possessing discrete energy levels associated with each component, is proposed in Figure 4. The

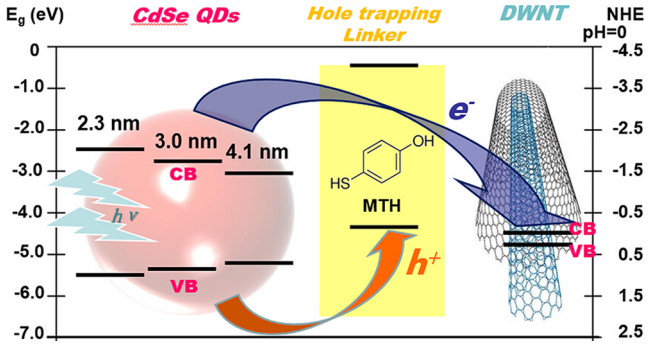

Figure 4. Energy diagram associated with DWNT−MTH-capped CdSe QD heterostructures incorporating various average QD sizes of 2.3, 3.0, and 4.1 nm, respectively. Plausible and reasonable charge-transfer pathways within these materials are indicated. It is expected that holes are being transferred from the valence bands of QDs to those of MTH linker molecules and end up being trapped in the process. Conversely, electrons are expected to tunnel into the conduction band of the DWNTs. e^-, electron; h^+, hole; CB, conduction band; and VB, valence band.

energy levels of CdSe QDs possessing different sizes as well as of the DWNTs have been calculated, based on previous papers.[58−61] The redox energy level of the thiophenol linker has been previously reported to be −0.006 V vs NHE,[62] which is situated at a higher energy as compared with the valence bands of all three CdSe QDs; hence, the linker is energetically favorable for hole transfer from the CdSe QDs. Upon excitation and photon absorption, an electron−hole pair exciton will form within the CdSe QDs. The photogenerated holes will then be efficiently trapped by the thiol groups within the MTH linker that is strongly adsorbed onto the CdSe QD surface, resulting in the creation of a thiol-based radical with the implication that two thiol-based radicals can react and combine to form a disulfide species.[18]

Because of the previously reported higher LUMO levels associated with these various thiol molecules,[22,63,64] electron transfer should occur at the interface between the CdSe QDs and the DWNTs, in which the intervening MTH linker molecule serves as an energetic barrier through which electrons can tunnel.[65,66] Hence, the difference between the conduction band energy levels of the CdSe QDs and of the DWNTs serves as a driving force for interfacial electron transfer.[67] Therefore, it is expected that ever smaller sizes of quantum confined QDs, possessing higher conduction band energy levels, should favor larger electron injection rates.

Nevertheless, it was noted that there was not a significant difference between the 3.0 and 4.1 nm diameter QD-based systems in terms of the C and O *K*-edges. Furthermore, we appeared to observe more charge transfer in the Cd M_3-edge for the composites incorporating 4.1 nm diameter QDs as opposed to 3.0 nm diameter QDs, although the smaller 3.0 nm diameter QDs with their higher conduction bands supposedly were more amenable to charge transfer.

One possible explanation for this aberration is the fact that we observed different QD coverage densities within these two systems. Specifically, as shown in Figure 1, the 4.1 nm diameter CdSe QDs evinced a noticeably higher coverage density (i.e., ∼ 1.5 times) as compared with their 3.0 nm diameter counterparts on the outer DWNT surface, thereby providing for greater interfacial contact areas as well as the potential possibility for additional pathways and channels for charge flow to occur from QDs to DWNTs with the net result that this intrinsic spatial, geometric consideration would dominate over the inherent electronic driving force associated with quantum confinement. The impact of QD coverage density upon the electron-transfer properties has also been specifically investigated using electrical transport measurements, as will be described later.

Raman Spectra. Raman spectra associated with pristine and oxidized DWNTs are displayed in Figure S5. The intensity ratio of the D band near 1340 cm^{-1} to the tangential mode (G band) near 1580 cm^{-1} (I_D/I_G) dramatically increases after the purification process (i.e., I_D/I_G = 0.04 for pristine DWNTs and 0.50 for purified DWNTs). The increase in the I_D/I_G ratio due to the purification process is expected, because the increased peak intensity associated with the D band can typically be attributed to damage and distortion of the intrinsic conjugated sp^2 carbon lattice, as well as to the presence of amorphous carbon[68] and other symmetry-breaking defects in the DWNTs generated during the oxidation and concomitant surface functionalization of DWNTs (i.e., formation of −COOH and other oxygenated species on the surfaces of our tubes).[69,70]

The tangential modes (G-bands) of the DWNT−MTH-capped CdSe QD composite heterostructures together with that of the DWNT−MTH control sample are collectively displayed in Figure 5. Each individual G band was treated as a

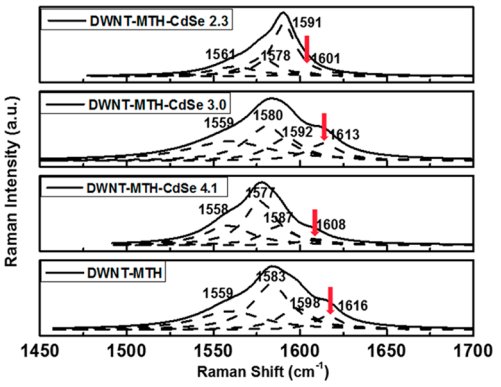

Figure 5. Raman G-band spectra measured at an excitation wavelength of 514 nm (2.41 eV) of a DWNT−MTH control sample as well as of DWNT−MTH-capped CdSe QD (with average constituent QD diameters of 2.3, 3.0, and 4.1 nm, respectively) heterostructures, generated by noncovalent $\pi-\pi$ stacking. The G^+ bands of the outer tubes for each sample are highlighted by the red arrows for clarity.

convolution of four Lorentzian components (i.e., the dashed curves). The two peaks at higher frequencies can be attributed to the G^+ and G^- bands of the semiconducting outer tube, whereas the other two peaks at lower frequencies correspond to the G^+ and G^- bands of the semiconducting inner tube. According to the Kataura plot,[71] the 2.41 eV excitation energy of the laser is in resonance with the E_{33}^S transition of a

DOI: 10.1021/acs.jpcc.5b08681
J. Phys. Chem. C 2015, 119, 26327−26338

semiconducting (S) outer tube as well as with the E_{33}^{S} transition of a semiconducting (S) inner tube. The fits of the sum of the Lorentzian peaks match well with previously reported G-band deconvolution data on DWNTs, possessing a S@S configuration.[72,73]

Upon deposition of CdSe QDs, all of the outer tube G^+ sub-bands (i.e., the peak with the highest frequency), which can be ascribed to the unresolved A_1 and E_1 tangential G^+ modes for the outer tubes,[74] evince an apparent peak downshift, an observation which can be potentially attributed to the G-band "softening", indicative of the expansion of C−C bonds upon *n*-type doping and suggestive of the presence of electron transfer from QDs in all three linker systems.[39,75] The observed downshifts in the frequency of the outer tube G^+-band of DWNT−MTH-capped CdSe QD heterostructures possessing QD sizes of 2.3, 3.0, and 4.1 nm are 15, 3, and 8 cm^{-1}, respectively. Moreover, the behavior associated with the downshift in the G^+_{outer} peak frequency gives rise to a trend similar to electron transfer that had been previously observed with the C *K*-edge and Cd M_3-edge NEXAFS spectra (i.e., QD diameters of 2.3 > 4.1 > 3.0 nm), again confirming the presence and extent of charge transfer. The fact that the inner tube G sub-bands barely alter after QD deposition is also consistent with a picture in which the charge from the QD donor is transferred to the outer tubes within the DWNT acceptor, which consequentially leads to a filling of those van Hove singularities (VHSs) within the conduction band of the nanotubes responsible for the observed Raman resonance.

Electrical Transport Measurements. Both NEXAFS and Raman spectroscopy data have confirmed the presence of electron transfer between CdSe QDs and the underlying DWNTs. Electrical transport measurements have been used to complement the optical data as well as to achieve additional insights into the impact of individual reaction parameters such as acid functionalization, QD sizes, and QD coverage densities. In total, more than 180 DWNT−MTH-capped CdSe QD heterostructure field-effect transistors (FETs) were characterized by a pulse measurement setup to reduce any hysteresis effect on the device[76] as well as to provide decent statistics that would allow for detecting any evident trends between variously chemically treated devices.

Specifically, exemplary subthreshold characteristics of a pristine DWNT and of an MTH-capped CdSe QD functionalized device obtained at V_{DS} = −0.5 V are shown in Figure 6 to illustrate the extraction process that was used to acquire insights into the impact of QD size and coverage density on the doping stage of DWNTs. For otherwise similar devices, the threshold voltage holds critical information about the doping stage of an FET and/or the amount of charge in the vicinity of the channel. Because extracting the actual threshold voltage V_{th} that defines the transition from the device off-state (where the current depends exponentially on the gate voltage) to the on-state that typically shows more of a power law dependence from experimental data is often challenging, we have used herein the change of V_{min}, i.e., the gate voltage at minimum current, as an indicator of the DWNT doping level.

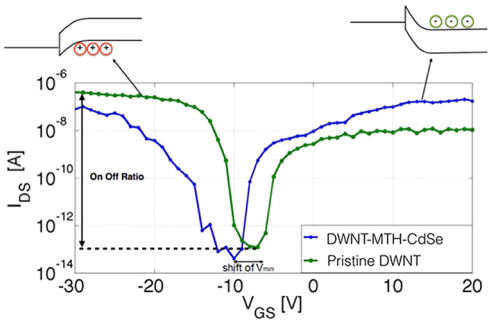

Figure 6. Sub-threshold characteristics of a pristine and MTH-functionalized DWNT FET measured at V_{DS} = −0.5 V. A clear shift of the minimum current point, i.e. V_{min}, is observed.

So-called ambipolar device characteristics are a result of electron transport through the nanotube conduction band at positive gate voltages and hole transport for negative gate voltages through the valence band. Of the above-mentioned total number of devices, those that show clear ambipolar behavior were selected for the extraction process that determines the gate voltage at which minimum current is reached as a qualitative measure of V_{th}. The process was discretely used for (a) pristine DWNTs, (b) DWNTs functionalized with MTH and CdSe QDs measuring 2.3 nm, (c) DWNTs functionalized with MTH and CdSe QDs possessing a diameter of 3.0 nm, as well as for (d) DWNTs functionalized with MTH and CdSe QDs with a diameter of 4.1 nm. It is worth mentioning here that all of the measurements have been carried out under dark conditions. Hence, the observed charge-transfer behavior is not associated with the photoinduced excitons,[77] but rather with possible work function differences among the various individual components in the system.

Figure 7 shows the actual V_{min} values extracted for pristine and various DWNT−MTH-capped CdSe QD heterostructures.

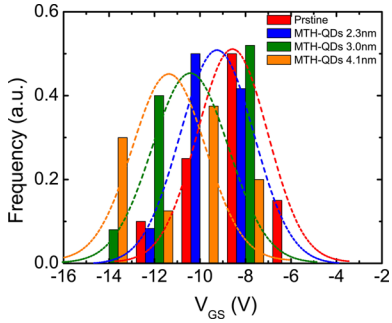

Figure 7. Distribution plot showing the trend of a shifted minimum current, V_{min}, for pristine and MTH-capped QD-functionalized DWNTs. The higher the level of QD decoration on the underlying DWNT surface, the more negative the V_{min}.

We note that while individual devices do demonstrate dissimilar V_{min} values, indicating varying doping levels, the large number of devices characterized in this study provides clear evidence of a doping trend between transistors of types a−d. In fact, our data suggest an increase in the *n*-doping level from a to d with the highest *n*-doping achieved in the DWNT−MTH-capped CdSe QD heterostructures, with average QD diameters measuring 4.1 nm, suggestive of the presence of the highest amount of charge generated in spatial proximity to the DWNTs. As has been pointed out before, the coverage of DWNTs varies with the choice of the QD size. We find that our transport results are consistent with the TEM-supported observation (Figure 1) that the average QD density varies from cases b (14 QDs/100 nm), c (16 QDs/100 nm), to d (27 QDs/100 nm).

DOI: 10.1021/acs.jpcc.5b08681
J. Phys. Chem. C 2015, 119, 26327−26338

We submit that it is the charge-transfer process from the MTH-capped CdSe QD system to the DWNT due to a smaller work function of the functionalized group as compared with the DWNT itself that creates the observed *n*-doping level, a finding that had not been previously reported. We also re-emphasize that the above statements are not related to the amount of charge transfer under illumination. Because all measurements were performed in the dark, no photoinduced electron transfer can be observed. Instead, the data indicate that the QD-ligand system once attached to the DWNT is no longer "charge neutral", an important fact that needs to be considered in the context of solar cell applications. To summarize, in the absence of laser illumination, systems possessing higher QD coverage densities lead to more charge transfer to the DWNT. Measurements of this series of DWNT−MTH-capped CdSe QD heterostructures in the presence of laser illumination are still under investigation in order to reveal additional insights into photoinduced charge transport.

It is also worth reinforcing our findings about DWNT functionalization from data associated with "on/off current ratios". When functionalizing DWNTs as opposed to single-wall carbon nanotubes (SWNTs) with the MTH-capped QD complex, the idea was to ensure the structural and electronic integrity of the inner carbon nanotube shell, while only breaking bonds associated with and attaching the ligands onto the outer shell of the DWNT. This approach appears to be a promising strategy for solar cell applications, because it ensures that excellent transport of charges through the inner shell of the system is preserved, even after functionalization of the outer tube shell has occurred. While the various optical methods presented above clearly indicate the successful attachment of the ligand−QD system, these measurements cannot unambiguously provide the desired information about the quality of transport through the DWNT system after functionalization. Therefore, herein we present for the first time a statistical study of on/off current ratios (see illustration in Figure 8) that provides initial insights into this topic.

While the fact that "on current" levels for functionalized DWNTs and pristine DWNTs are similar (as shown in Figure 6) and already provide initial evidence of the absence of a severely damaged tube channel, Figure 8 further evaluates the specific impact of the tube functionalization by evaluating the distribution of experimentally measured I_{on}/I_{off} values for a large number of three-terminal devices. For pristine DWNT FETs, the expectation is that on/off current ratios are rather small, consistent with the notion that the outer shell of a DWNT with its larger diameter exhibits a smaller band gap that results in a higher off-current as compared with a SWNT. Groups have recently reported[78,79] on/off current ratios of about 3 and 4 orders of magnitude, consistent with this statement.

Our results indicate that pristine DWNT FETs exhibit I_{on}/I_{off} values larger than 2 in only about 13% of all cases, and none of these devices characterized achieved an on/off ratio of 8. On the other hand, a much larger number of devices, i.e., 22% of MTH-capped CdSe QD-functionalized DWNTs exhibited $\log(I_{on}/I_{off}) > 2$, and a small number of these devices even attained on/off current ratios of as large as 8 orders of magnitude (cf. Figure 8). This interesting observation can be understood in the context of the above intuitive argument of breaking only the outer, external carbon nanotube shell when attaching the MTH-capped CdSe QDs onto the DWNT structure. In fact, we find that in 34% of all SWNT FETs, on/off current ratios larger than 2 orders of magnitude are obtained and values as high as 8 orders of magnitude are achievable in some FETs (see lower distribution plot in Figure 8). Our experimental data clearly suggest that the device behavior of DWNTs is becoming more similar to pristine SWNT FETs after functionalization, thereby confirming the validity of the intuitive picture.

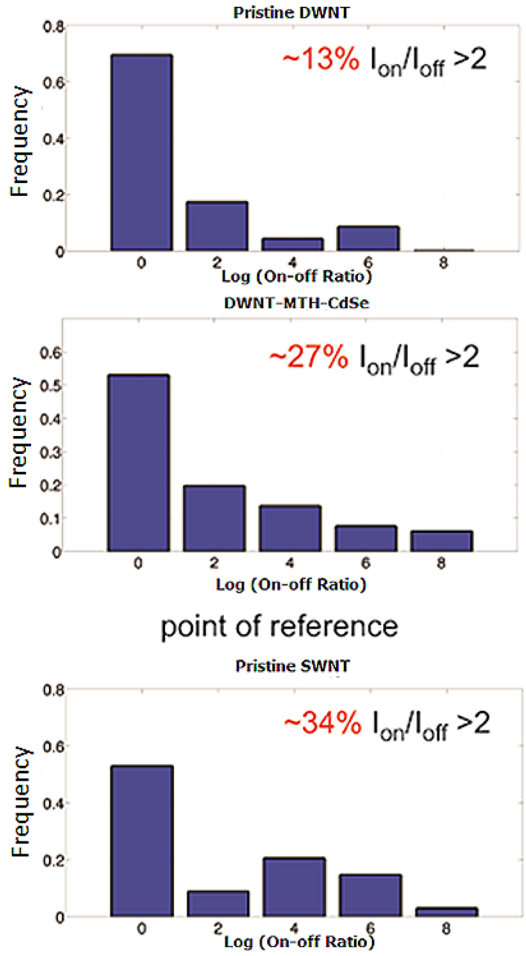

Figure 8. On/off-current distribution for pristine and functionalized carbon nanotubes. A larger portion of functionalized DWNTs shows an on/off-current ratio larger than 2 as compared with pristine DWNTs.

CONCLUSIONS

DWNT−MTH-capped CdSe QD heterostructures, possessing average QD diameters ranging from 2.3, 3.0, to 4.1 nm, respectively, have been successfully synthesized using a facile noncovalent $\pi-\pi$ attachment approach through the mediation of MTH linker. TEM and HRTEM images have indicated that the 4.1 nm diameter MTH-capped CdSe QDs are quantitatively more numerous as compared with their smaller-sized counterparts in terms of coverage density on the underlying DWNT surface.

With a collective analysis of both NEXAFS and Raman spectra, plausible evidence for electron transfer has been proposed for all the DWNT−MTH-capped CdSe QD heterostructures. Specifically, analysis of the NEXAFS spectra of DWNT−MTH-capped CdSe QD heterostructures incorporating different QD sizes confirms that the interfacial electron transfer falls within the "normal" Marcus theory region, wherein

DOI: 10.1021/acs.jpcc.5b08681
J. Phys. Chem. C 2015, 119, 26327−26338

the heterostructure possessing the smallest QD size (i.e., 2.3 nm) gives rise to the largest driving force for charge transfer. The heterostructure possessing larger 4.1 nm diameter QDs yielded anomalously greater charge-transfer behavior with respect to that containing 3.0 nm diameter QDs, an observation which can be ascribed to differential coverage densities onto the underlying DWNT templates.

Complementary Raman investigation at 2.41 eV excitation evinced an evident downshift of the outer tube G^+-band, thereby suggesting that CdSe QDs serve as electron donors, wherein electrons are predominantly transferred to the outer tubes in DWNTs in all three as-synthesized DWNT−MTH-capped CdSe QD heterostructures, which led not only to a filling of the Van Hove singularities of the conduction band but also to a further "softening" of the C−C bond, thereby shifting the G^+-band to lower frequencies. We note that this downshift in the G^+_{outer} peak frequency gives rise to a similar trend to what has been previously noted with electron transfer in the NEXAFS spectra (QD diameters of 2.3 > 4.1 > 3.0 nm), again confirming the presence and extent of charge transfer.

The electrical transport measurements obtained in the absence of illumination, which serves as a complementary measurement to the aforementioned optical data, indicated that the MTH-capped QDs once attached onto the DWNTs are no longer "charge neutral" and further correlated the idea of *n*-doping, i.e., the presence of electron transfer under "dark" conditions from the QDs to DWNTs which is essentially dependent upon the QD coverage densities, as corroborated by interpretable changes in threshold voltage characteristics. The on−off ratios from the FETs further confirmed that the acid treatment used selectively functionalizes the outer tubes of the DWNTs and hence preserves the electronic integrity of the inner tubes.

Therefore, the cumulative NEXAFS, Raman, and electrical transport studies present in this work have highlighted the presence of electron transfer in the DWNT−MTH-capped CdSe QD heterostructures both under photonic excitation as well as under "dark" illumination conditions. Moreover, our studies offer a reasonable capability and path forward to tune and facilitate charge transfer to DWNTs via size and coverage density control of immobilized CdSe QDs. Such findings should shed light upon the connection between architectural design and control of charge separation within the context of QD-based solar cell regimes.

■ ASSOCIATED CONTENT

Supporting Information

The Supporting Information is available free of charge on the ACS Publications website at DOI: 10.1021/acs.jpcc.5b08681.

Additional data on electron microscopy as well as relevant UV−visible, infrared, NEXAFS, and Raman spectroscopy results, coupled with appropriate discussion (PDF).

■ AUTHOR INFORMATION

Corresponding Author

*E-mail: stanislaus.wong@stonybrook.edu; sswong@bnl.gov.

Notes

The authors declare no competing financial interest.

■ ACKNOWLEDGMENTS

Research (including support for L.W., J.H., Y.Z., R.Z., H.L., J.A., and S.S.W.) was provided by the U.S. Department of Energy, Basic Energy Sciences, Materials Sciences and Engineering Division. NEXAFS experiments were carried out at the National Synchrotron Light Source at Brookhaven National Laboratory, which is supported by the U.S. Department of Energy under Contracts DE-AC02-98CH10886 and DE-SC-00112704. Raman data were acquired at Stony Brook University's Nano-Raman Molecular Imaging Laboratory (NARMIL), established with NSF MRI Grant OCE-1336724. Certain commercial names used in this manuscript are for illustration purposes and do not constitute an endorsement by the National Institute of Standards and Technology.

■ REFERENCES

(1) Peng, X.; Sfeir, M. Y.; Zhang, F.; Misewich, J. A.; Wong, S. S. Covalent Synthesis and Optical Characterization of Double-Walled Carbon Nanotube-Nanocrystal Heterostructures. *J. Phys. Chem. C* **2010**, *114*, 8766−8733.

(2) Schulz-Drost, C.; Sgobba, V.; Gerhards, C.; Leubner, S.; Calderon, R. M. K.; Ruland, A.; Guldi, D. M. Innovative Inorganic-Organic Nanohybrid Materials: Coupling Quantum Dots to Carbon Nanotubes. *Angew. Chem., Int. Ed.* **2010**, *49*, 6425−6429.

(3) Wang, D. F.; Baral, J. K.; Zhao, H. G.; Gonfa, B. A.; Truong, V. V.; El Khakani, M. A.; Izquierdo, R.; Ma, D. L. Controlled Fabrication of PbS Quantum-Dot/Carbon-Nanotube Nanoarchitecture and Its Significant Contribution to near-Infrared Photon-to-Current Conversion. *Adv. Funct. Mater.* **2011**, *21*, 4010−4018.

(4) Reiss, P.; Protiere, M.; Li, L. Core/Shell Semiconductor Nanocrystals. *Small* **2009**, *5*, 154−168.

(5) Zhang, L. H.; Shi, E. Z.; Li, Z.; Li, P. X.; Jia, Y.; Ji, C. Y.; Wei, J. Q.; Wang, K. L.; Zhu, H. W.; Wu, D. H.; et al. Wire-Supported CdSe Nanowire Array Photoelectrochemical Solar Cells. *Phys. Chem. Chem. Phys.* **2012**, *14*, 3583−3588.

(6) Peng, X. H.; Wong, S. S. Controlling Nanocrystal Density and Location on Carbon Nanotube Templates. *Chem. Mater.* **2009**, *21*, 682−694.

(7) Peng, X. H.; Sfeir, M. Y.; Zhang, F.; Misewich, J. A.; Wong, S. S. Covalent Synthesis and Optical Characterization of Double-Walled Carbon Nanotube-Nanocrystal Heterostructures. *J. Phys. Chem. C* **2010**, *114*, 8766−8773.

(8) Banerjee, S.; Wong, S. S. Formation of CdSe Nanocrystals onto Oxidized, Ozonized Single-Walled Carbon Nanotube Surfaces. *Chem. Commun.* **2004**, 1866−1867.

(9) Peng, X. H.; Misewich, J. A.; Wong, S. S.; Sfeir, M. Y. Efficient Charge Separation in Multidimensional Nanohybrids. *Nano Lett.* **2011**, *11*, 4562−4568.

(10) Newton, J. C.; Ramasamy, K.; Mandal, M.; Joshi, G. K.; Kumbhar, A.; Sardar, R. Low-Temperature Synthesis of Magic-Sized CdSe Nanoclusters: Influence of Ligands on Nanocluster Growth and Photophysical Properties. *J. Phys. Chem. C* **2012**, *116*, 4380−4389.

(11) Ning, Z.; Voznyy, O.; Pan, J.; Hoogland, S.; Adinolfi, V.; Xu, J.; Li, M.; Kirmani, A. R.; Sun, J.-P.; Minor, J.; et al. Air-Stable N-Type Colloidal Quantum Dot Solids. *Nat. Mater.* **2014**, *13*, 822−828.

(12) Fischer, A.; Rollny, L.; Pan, J.; Carey, G. H.; Thon, S. M.; Hoogland, S.; Voznyy, O.; Zhitomirsky, D.; Kim, J. Y.; Bakr, O. M.; et al. Directly Deposited Quantum Dot Solids Using a Colloidally Stable Nanoparticle Ink. *Adv. Mater.* **2013**, *25*, 5742−5749.

(13) Anderson, N. C.; Hendricks, M. P.; Choi, J. J.; Owen, J. S. Ligand Exchange and the Stoichiometry of Metal Chalcogenide Nanocrystals: Spectroscopic Observation of Facile Metal-Carboxylate Displacement and Binding. *J. Am. Chem. Soc.* **2013**, *135*, 18536−18548.

(14) Mora-Sero, I.; Bertoluzzi, L.; Gonzalez-Pedro, V.; Gimenez, S.; Fabregat-Santiago, F.; Kemp, K. W.; Sargent, E. H.; Bisquert, J. Selective Contacts Drive Charge Extraction in Quantum Dot Solids

Via Asymmetry in Carrier Transfer Kinetics. *Nat. Commun.* **2013**, *4*, 3272-1−3272-8.
(15) Tang, J.; Kemp, K. W.; Hoogland, S.; Jeong, K. S.; Liu, H.; Levina, L.; Furukawa, M.; Wang, X. H.; Debnath, R.; Cha, D. K.; et al. Colloidal-Quantum-Dot Photovoltaics Using Atomic-Ligand Passivation. *Nat. Mater.* **2011**, *10*, 765−771.
(16) Wang, L.; Han, J.; Hoy, J.; Hu, F.; Liu, H. Q.; Gentleman, M. M.; Sfeir, M. Y.; Misewich, J. A.; Wong, S. S. Probing Differential Optical and Coverage Behavior in Nanotube-Nanocrystal Heterostructures Synthesized by Covalent Versus Non-Covalent Approaches. *Dalton Trans.* **2014**, *43*, 7480−7490.
(17) Liu, I. S.; Lo, H.-H.; Chien, C.-T.; Lin, Y.-Y.; Chen, C.-W.; Chen, Y.-F.; Su, W.-F.; Liou, S.-C. Enhancing Photoluminescence Quenching and Photoelectric Properties of CdSe Quantum Dots with Hole Accepting Ligands. *J. Mater. Chem.* **2008**, *18*, 675−682.
(18) Wuister, S. F.; de Mello Donegá, C.; Meijerink, A. Influence of Thiol Capping on the Exciton Luminescence and Decay Kinetics of CdTe and CdSe Quantum Dots. *J. Phys. Chem. B* **2004**, *108*, 17393−17397.
(19) Yu, K.; Lu, G.; Chen, K.; Mao, S.; Kim, H.; Chen, J. Controllable Photoelectron Transfer in CdSe Nanocrystal-Carbon Nanotube Hybrid Structures. *Nanoscale* **2012**, *4*, 742−746.
(20) Robel, I.; Bunker, B. A.; Kamat, P. V. Single-Walled Carbon Nanotube-CdS Nanocomposites as Light-Harvesting Assemblies: Photoinduced Charge-Transfer Interactions. *Adv. Mater.* **2005**, *17*, 2458−2463.
(21) Hansen, T.; Zidek, K.; Zheng, K. B.; Abdellah, M.; Chabera, P.; Persson, P.; Pullerits, T. Orbital Topology Controlling Charge Injection in Quantum-Dot-Sensitized Solar Cells. *J. Phys. Chem. Lett.* **2014**, *5*, 1157−1162.
(22) Hines, D. A.; Forrest, R. P.; Corcelli, S. A.; Kamat, P. V. Predicting the Rate Constant of Electron Tunneling Reactions at the CdSe-TiO_2 Interface. *J. Phys. Chem. B* **2015**, *119*, 7439−7446.
(23) Weaver, J. E.; Dasari, M. R.; Datar, A.; Talapatra, S.; Kohli, P. Investigating Photoinduced Charge Transfer in Carbon Nanotube-Perylene-Quantum Dot Hybrid Nanocomposites. *ACS Nano* **2010**, *4*, 6883−6893.
(24) Zhu, N.; Zheng, K.; Karki, K. J.; Abdellah, M.; Zhu, Q.; Carlson, S.; Haase, D.; Žídek, K.; Ulstrup, J.; Canton, S. E.; et al. Sandwiched Confinement of Quantum Dots in Graphene Matrix for Efficient Electron Transfer and Photocurrent Production. *Sci. Rep.* **2015**, *5*, 9860-1−9860-14.
(25) Hahner, G. Near Edge X-ray Absorption Fine Structure Spectroscopy as a Tool to Probe Electronic and Structural Properties of Thin Organic Films and Liquids. *Chem. Soc. Rev.* **2006**, *35*, 1244−1255.
(26) De Jesus, L. R.; Dennis, R. V.; Depner, S. W.; Jaye, C.; Fischer, D. A.; Banerjee, S. Inside and Outside: X-ray Absorption Spectroscopy Mapping of Chemical Domains in Graphene Oxide. *J. Phys. Chem. Lett.* **2013**, *4*, 3144−3151.
(27) Kuznetsova, A.; Popova, I.; Yates, J. T.; Bronikowski, M. J.; Huffman, C. B.; Liu, J.; Smalley, R. E.; Hwu, H. H.; Chen, J. G. G. Oxygen-Containing Functional Groups on Single-Wall Carbon Nanotubes: NEXAFS and Vibrational Spectroscopic Studies. *J. Am. Chem. Soc.* **2001**, *123*, 10699−10704.
(28) Wang, Z.; Wu, L.; Zhou, J.; Cai, W.; Shen, B.; Jiang, Z. Magnetite Nanocrystals on Multiwalled Carbon Nanotubes as a Synergistic Microwave Absorber. *J. Phys. Chem. C* **2013**, *117*, 5446−5452.
(29) Winter, A. D.; Larios, E.; Alamgir, F. M.; Jaye, C.; Fischer, D. A.; Omastova, M.; Campo, E. M. Thermo-Active Behavior of Ethylene-Vinyl Acetate|Multiwall Carbon Nanotube Composites Examined by in Situ near-Edge X-ray Absorption Fine-Structure Spectroscopy. *J. Phys. Chem. C* **2014**, *118*, 3733−3741.
(30) Zhou, J. G.; Fang, H. T.; Maley, J. M.; Ko, J. Y. P.; Murphy, M.; Chu, Y.; Sammynaiken, R.; Sham, T. K. An X-ray Absorption, Photoemission, and Raman Study of the Interaction between SnO_2 Nanoparticle and Carbon Nanotube. *J. Phys. Chem. C* **2009**, *113*, 6114−6117.
(31) Koroteev, V. O.; Bulusheva, L. G.; Asanov, I. P.; Shlyakhova, E. V.; Vyalikh, D. V.; Okotrub, A. V. Charge Transfer in the MoS_2/Carbon Nanotube Composite. *J. Phys. Chem. C* **2011**, *115*, 21199−21204.
(32) Yueh, C. L.; Jan, J. C.; Chiou, J. W.; Pong, W. F.; Tsai, M. H.; Chang, Y. K.; Chen, Y. Y.; Lee, Y. F.; Tseng, P. K.; Wei, S. L.; et al. Electronic Structure of the Fe-Layer-Catalyzed Carbon Nanotubes Studied by X-ray-Absorption Spectroscopy. *Appl. Phys. Lett.* **2001**, *79*, 3179−3181.
(33) Chen, G. G.; Bandow, S.; Margine, E. R.; Nisoli, C.; Kolmogorov, A. N.; Crespi, V. H.; Gupta, R.; Sumanasekera, G. U.; Iijima, S.; Eklund, P. C. Chemically Doped Double-Walled Carbon Nanotubes: Cylindrical Molecular Capacitors. *Phys. Rev. Lett.* **2003**, *90*, 257403.
(34) do Nascimento, G. M.; Hou, T.; Kim, Y. A.; Muramatsu, H.; Hayashi, T.; Endo, M.; Akuzawa, N.; Dresselhaus, M. S. Double-Wall Carbon Nanotubes Doped with Different Br_2 Doping Levels: A Resonance Raman Study. *Nano Lett.* **2008**, *8*, 4168−4172.
(35) do Nascimento, G. M.; Hou, T.; Kim, Y. A.; Muramatsu, H.; Hayashi, T.; Endo, M.; Akuzawa, N.; Dresselhaus, M. S. Comparison of the Resonance Raman Behavior of Double-Walled Carbon Nanotubes Doped with Bromine or Iodine Vapors. *J. Phys. Chem. C* **2009**, *113*, 3934−3938.
(36) Cambedouzou, J.; Sauvajol, J. L.; Rahmani, A.; Flahaut, E.; Peigney, A.; Laurent, C. Raman Spectroscopy of Iodine-Doped Double-Walled Carbon Nanotubes. *Phys. Rev. B: Condens. Matter Mater. Phys.* **2004**, *69*, 235422.
(37) do Nascimento, G. M.; Hou, T.; Kim, Y. A.; Muramatsu, H.; Hayashi, T.; Endo, M.; Akuzawa, N.; Dresselhaus, M. S. Behavior of the High Frequency Raman Modes of Double-Wall Carbon Nanotubes after Doping with Bromine or Iodine Vapors. *Carbon* **2011**, *49*, 3585−3596.
(38) Souza Filho, A. G.; Endo, M.; Muramatsu, H.; Hayashi, T.; Kim, Y. A.; Barros, E. B.; Akuzawa, N.; Samsonidze, G. G.; Saito, R.; Dresselhaus, M. S. Resonance Raman Scattering Studies in Br_2-Adsorbed Double-Wall Carbon Nanotubes. *Phys. Rev. B: Condens. Matter Mater. Phys.* **2006**, *73*, 235413.
(39) Li, Y. F.; Hatakeyama, R.; Kaneko, T.; Izumida, T.; Okada, T.; Kato, T. Synthesis and Electronic Properties of Ferrocene-Filled Double-Walled Carbon Nanotubes. *Nanotechnology* **2006**, *17*, 4143−4147.
(40) Zhang, L. H.; Jia, Y.; Wang, S. S.; Li, Z.; Ji, C. Y.; Wei, J. Q.; Zhu, H. W.; Wang, K. L.; Wu, D. H.; Shi, E. Z.; et al. Carbon Nanotube and CdSe Nanobelt Schottky Junction Solar Cells. *Nano Lett.* **2010**, *10*, 3583−3589.
(41) Bang, J. H.; Kamat, P. V. Quantum Dot Sensitized Solar Cells. A Tale of Two Semiconductor Nanocrystals: CdSe and CdTe. *ACS Nano* **2009**, *3*, 1467−1476.
(42) Bolotin, K. I.; Sikes, K. J.; Jiang, Z.; Klima, M.; Fudenberg, G.; Hone, J.; Kim, P.; Stormer, H. L. Ultrahigh Electron Mobility in Suspended Graphene. *Solid State Commun.* **2008**, *146*, 351−355.
(43) Zhao, J.; Cao, M.; Cheng, B.; Wu, G.; Guo, H.; Ai, Y.; Su, X.; Xiao, Y.; Lei, S. Carbon-Encapsulated CdSe Quantum Dot Inorganic Hybrid Nanobelts for High Performance Photoelectronic Devices Based on the Efficient Separation and Transfer of Photoinduced Holes. *J. Mater. Chem. C* **2015**, *3*, 2471−2478.
(44) Qu, L. H.; Peng, X. G. Control of Photoluminescence Properties of CdSe Nanocrystals in Growth. *J. Am. Chem. Soc.* **2002**, *124*, 2049−2055.
(45) Ravel, B.; Newville, M. Athena, Artemis, Hephaestus: Data Analysis for X-ray Absorption Spectroscopy Using Ifeffit. *J. Synchrotron Radiat.* **2005**, *12*, 537−541.
(46) Liu, C.; Lee, S.; Su, D.; Zhang, Z.; Pfefferle, L.; Haller, G. L. Synthesis and Characterization of Nanocomposites with Strong Interfacial Interaction: Sulfated ZrO_2 Nanoparticles Supported on Multiwalled Carbon Nanotubes. *J. Phys. Chem. C* **2012**, *116*, 21742−21752.
(47) Banerjee, S.; Hemraj-Benny, T.; Balasubramanian, M.; Fischer, D. A.; Misewich, J. A.; Wong, S. S. Surface Chemistry and Structure of

DOI: 10.1021/acs.jpcc.5b08681
J. Phys. Chem. C 2015, 119, 26327−26338

Purified, Ozonized, Multiwalled Carbon Nanotubes Probed by NEXAFS and Vibrational Spectroscopies. *ChemPhysChem* **2004**, *5*, 1416−1422.
(48) Leon, V.; Parret, R.; Almairac, R.; Alvarez, L.; Babaa, M. R.; Doyle, B. P.; Ienny, P.; Parent, P.; Zahab, A.; Bantignies, J. L. Spectroscopic Study of Double-Walled Carbon Nanotube Functionalization for Preparation of Carbon Nanotube/Epoxy Composites. *Carbon* **2012**, *50*, 4987−4994.
(49) Lee, J. R. I.; Meulenberg, R. W.; Hanif, K. M.; Mattoussi, H.; Klepeis, J. E.; Terminello, L. J.; van Buuren, T. Experimental Observation of Quantum Confinement in the Conduction Band of CdSe Quantum Dots. *Phys. Rev. Lett.* **2007**, *98*, 146803.
(50) Wright, J. T.; Meulenberg, R. W. Modification of the Conduction Band Edge Energy Via Hybridization in Quantum Dots. *Appl. Phys. Lett.* **2012**, *101*, 193104.
(51) Liang, Y.; Wang, H.; Zhou, J.; Li, Y.; Wang, J.; Regier, T.; Dai, H. Covalent Hybrid of Spinel Manganese−Cobalt Oxide and Graphene as Advanced Oxygen Reduction Electrocatalysts. *J. Am. Chem. Soc.* **2012**, *134*, 3517−3523.
(52) Marcus, R. A. On the Theory of Oxidation-Reduction Reactions Involving Electron Transfer. *J. Chem. Phys.* **1956**, *24*, 966−978.
(53) Marcus, R. A. Chemical and Electrochemical Electron-Transfer Theory. *Annu. Rev. Phys. Chem.* **1964**, *15*, 155−196.
(54) Tarafder, K.; Surendranath, Y.; Olshansky, J. H.; Alivisatos, A. P.; Wang, L. W. Hole Transfer Dynamics from a CdSe/CdS Quantum Rod to a Tethered Ferrocene Derivative. *J. Am. Chem. Soc.* **2014**, *136*, 5121−5131.
(55) Tafen, D.; Prezhdo, O. V. Size and Temperature Dependence of Electron Transfer between CdSe Quantum Dots and a TiO_2 Nanobelt. *J. Phys. Chem. C* **2015**, *119*, 5639−5647.
(56) Tvrdy, K.; Frantsuzov, P. A.; Kamat, P. V. Photoinduced Electron Transfer from Semiconductor Quantum Dots to Metal Oxide Nanoparticles. *Proc. Natl. Acad. Sci. U. S. A.* **2011**, *108*, 29−34.
(57) Robel, I.; Kuno, M.; Kamat, P. V. Size-Dependent Electron Injection from Excited CdSe Quantum Dots into TiO_2 Nanoparticles. *J. Am. Chem. Soc.* **2007**, *129*, 4136−4137.
(58) Meulenberg, R. W.; Lee, J. R.; Wolcott, A.; Zhang, J. Z.; Terminello, L. J.; van Buuren, T. Determination of the Exciton Binding Energy in CdSe Quantum Dots. *ACS Nano* **2009**, *3*, 325−330.
(59) Mintmire, J. W.; White, C. T. Electronic and Structural Properties of Carbon Nanotubes. *Carbon* **1995**, *33*, 893−902.
(60) Shan, B.; Cho, K. First-Principles Study of Work Functions of Double-Wall Carbon Nanotubes. *Phys. Rev. B: Condens. Matter Mater. Phys.* **2006**, *73*, 081401.
(61) Jasieniak, J.; Califano, M.; Watkins, S. E. Size-Dependent Valence and Conduction Band-Edge Energies of Semiconductor Nanocrystals. *ACS Nano* **2011**, *5*, 5888−5902.
(62) Liu, I. S.; Lo, H. H.; Chien, C. T.; Lin, Y. Y.; Chen, C. W.; Chen, Y. F.; Su, W. F.; Liou, S. C. Enhancing Photoluminescence Quenching and Photoelectric Properties of CdSe Quantum Dots with Hole Accepting Ligands. *J. Mater. Chem.* **2008**, *18*, 675−682.
(63) Li, J.; Zhang, M. Atomic Insights into Adsorption of Thiophenol Derivatives as Corrosion Inhibitors for Mild Steel in Hydrochloric Acid Solution. *Mater. Res. Innovations* **2014**, *18*, 38−42.
(64) Kalimuthu, P.; Sivanesan, A.; John, S. A. Charge-Transfer Interaction of Aromatic Thiols with 2,3-Dichloro-5,6-Dicyano-*p*-Benzoquinone: Spectral and Quantum Mechanical Studies. *J. Phys. Chem. A* **2007**, *111*, 12086−12092.
(65) Liu, Y.; Gibbs, M.; Puthussery, J.; Gaik, S.; Ihly, R.; Hillhouse, H. W.; Law, M. Dependence of Carrier Mobility on Nanocrystal Size and Ligand Length in PbSe Nanocrystal Solids. *Nano Lett.* **2010**, *10*, 1960−1969.
(66) Wang, H.; McNellis, E. R.; Kinge, S.; Bonn, M.; Canovas, E. Tuning Electron Transfer Rates through Molecular Bridges in Quantum Dot Sensitized Oxides. *Nano Lett.* **2013**, *13*, 5311−5315.
(67) Kongkanand, A.; Tvrdy, K.; Takechi, K.; Kuno, M.; Kamat, P. V. Quantum Dot Solar Cells. Tuning Photoresponse through Size and Shape Control of CdSe-TiO_2 Architecture. *J. Am. Chem. Soc.* **2008**, *130*, 4007−4015.
(68) Osswald, S.; Flahaut, E.; Ye, H.; Gogotsi, Y. Elimination of D-Band in Raman Spectra of Double-Wall Carbon Nanotubes by Oxidation. *Chem. Phys. Lett.* **2005**, *402*, 422−427.
(69) Jung, G. B.; Myung, Y.; Park, J.; Maeng, I.; Son, J.-H. Terahertz Spectroscopy of Platinum, Copper Sulfide, and Tin Oxide Nanocrystals-Carbon Nanotube Hybrid Nanostructures. In 34th International Conference on Infrared, Millimeter, and Terahertz Waves, 2009 (IRMMW-THz 2009), Busan, Sept. 21−25, 2009; pp 1−2. DOI: 10.1109/ICIMW.2009.5325644.
(70) Campidelli, S.; Sooambar, C.; Lozano Diz, E.; Ehli, C.; Guldi, D. M.; Prato, M. Dendrimer-Functionalized Single-Wall Carbon Nanotubes: Synthesis, Characterization, and Photoinduced Electron Transfer. *J. Am. Chem. Soc.* **2006**, *128*, 12544−12552.
(71) Kataura, H.; Kumazawa, Y.; Maniwa, Y.; Umezu, I.; Suzuki, S.; Ohtsuka, Y.; Achiba, Y. Optical Properties of Single-Wall Carbon Nanotubes. *Synth. Met.* **1999**, *103*, 2555−2558.
(72) Bandow, S.; Chen, G.; Sumanasekera, G. U.; Gupta, R.; Yudasaka, M.; Iijima, S.; Eklund, P. C. Diameter-Selective Resonant Raman Scattering in Double-Wall Carbon Nanotubes. *Phys. Rev. B: Condens. Matter Mater. Phys.* **2002**, *66*, 075416.
(73) Villalpando-Paez, F.; Son, H.; Nezich, D.; Hsieh, Y. P.; Kong, J.; Kim, Y. A.; Shimamoto, D.; Muramatsu, H.; Hayashi, T.; Endo, M.; et al. Raman Spectroscopy Study of Isolated Double-Walled Carbon Nanotubes with Different Metallic and Semiconducting Configurations. *Nano Lett.* **2008**, *8*, 3879−3886.
(74) Rahmani, A.; Sauvajol, J. L.; Rols, S.; Benoit, C. Nonresonant Raman Spectrum in Infinite and Finite Single-Wall Carbon Nanotubes. *Phys. Rev. B: Condens. Matter Mater. Phys.* **2002**, *66*, 125404.
(75) Rauf, H.; Pichler, T.; Pfeiffer, R.; Simon, F.; Kuzmany, H.; Popov, V. N. Detailed Analysis of the Raman Response of N-Doped Double-Wall Carbon Nanotubes. *Phys. Rev. B: Condens. Matter Mater. Phys.* **2006**, *74*, 235419.
(76) Estrada, D.; Dutta, S.; Liao, A.; Pop, E. Reduction of Hysteresis for Carbon Nanotube Mobility Measurements Using Pulsed Characterization. *Nanotechnology* **2010**, *21*, 085702-1−087702-7.
(77) Huynh, W. U.; Dittmer, J. J.; Teclemariam, N.; Milliron, D. J.; Alivisatos, A. P.; Barnham, K. W. J. Charge Transport in Hybrid Nanorod-Polymer Composite Photovoltaic Cells. *Phys. Rev. B: Condens. Matter Mater. Phys.* **2003**, *67*, 115326.
(78) Green, A. A.; Hersam, M. C. Properties and Application of Double-Walled Carbon Nanotubes Sorted by Outer-Wall Electronic Type. *ACS Nano* **2011**, *5*, 1459−1467.
(79) Liu, K.; Wang, W.; Xu, Z.; Bai, X.; Wang, E.; Yao, Y.; Zhang, J.; Liu, Z. Chirality-Dependent Transport Properties of Double-Walled Nanotubes Measured in Situ on Their Field-Effect Transistors. *J. Am. Chem. Soc.* **2009**, *131*, 62−63.

DOI: 10.1021/acs.jpcc.5b08681
J. Phys. Chem. C 2015, 119, 26327−26338